

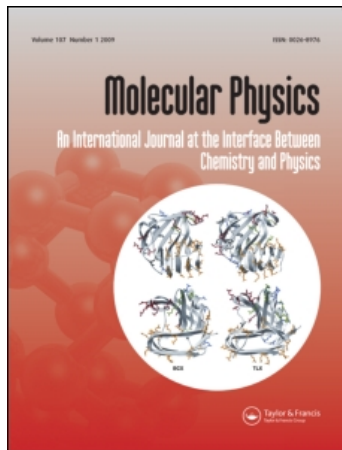
This article was downloaded by: [Messina, Rene]

On: 16 May 2011

Access details: Access Details: [subscription number 937058834]

Publisher Taylor & Francis

Informa Ltd Registered in England and Wales Registered Number: 1072954 Registered office: Mortimer House, 37-41 Mortimer Street, London W1T 3JH, UK



Molecular Physics

Publication details, including instructions for authors and subscription information:

<http://www.informaworld.com/smpp/title~content=t713395160>

Heterogeneous crystallization near structured walls in quenched two-dimensional binary colloidal suspensions

Lahcen Assoud^a; René Messina^a; Hartmut Löwen^a

^a Institut für Theoretische Physik II: Weiche Materie, Heinrich-Heine-Universität Düsseldorf, D-40225 Düsseldorf, Germany

Online publication date: 29 April 2011

To cite this Article Assoud, Lahcen , Messina, René and Löwen, Hartmut(2011) 'Heterogeneous crystallization near structured walls in quenched two-dimensional binary colloidal suspensions', Molecular Physics, 109: 7, 1385 – 1391

To link to this Article: DOI: 10.1080/00268976.2011.562871

URL: <http://dx.doi.org/10.1080/00268976.2011.562871>

PLEASE SCROLL DOWN FOR ARTICLE

Full terms and conditions of use: <http://www.informaworld.com/terms-and-conditions-of-access.pdf>

This article may be used for research, teaching and private study purposes. Any substantial or systematic reproduction, re-distribution, re-selling, loan or sub-licensing, systematic supply or distribution in any form to anyone is expressly forbidden.

The publisher does not give any warranty express or implied or make any representation that the contents will be complete or accurate or up to date. The accuracy of any instructions, formulae and drug doses should be independently verified with primary sources. The publisher shall not be liable for any loss, actions, claims, proceedings, demand or costs or damages whatsoever or howsoever caused arising directly or indirectly in connection with or arising out of the use of this material.

INVITED ARTICLE

Heterogeneous crystallization near structured walls in quenched two-dimensional binary colloidal suspensions

Lahcen Assoud, René Messina* and Hartmut Löwen

*Institut für Theoretische Physik II: Weiche Materie, Heinrich-Heine-Universität Düsseldorf,
Universitätsstraße 1, D-40225 Düsseldorf, Germany*

(Received 5 November 2010; final version received 4 February 2011)

Crystallization near structured substrates is explored by extensive Brownian dynamics computer simulations of two-dimensional equimolar binary colloidal suspensions. The particles are interacting via repulsive dipole–dipole forces. The two species have different (big and small) dipole moments which are tunable by an external magnetic field. A quench is realized by a sudden drastic increase of the magnetic field which formally corresponds to a quench to zero temperature. The structured walls are modelled by fixed particles on an alternating binary equimolar square lattice which is cut along the (10) direction. Two situations are studied and compared where the outermost layer of fixed particles either consists of big or of small dipolar particles. Both of these structures favour local crystallites which pick up the square symmetry of the substrate. After the quench the equilibrium state is an alternating square lattice which coincides exactly with that imposed by the external wall. The relaxation behaviour following the quench is explored. The amount of local crystallites with triangular and square symmetry is monitored as a function of time for different initial temperatures. It is found that the number and structure of crystallites near the walls strongly depend on the wall pattern. Even though local square structures are favoured energetically and the equilibrium state is an alternating square lattice, the number of triangular crystallites close to the wall which has outermost fixed small particles is significantly higher than in the unconfined case. The actual number of triangular clusters depends on the depth of the quench. This effect is not contained in classical nucleation theory.

Keywords: heterogeneous crystallization; nucleation; colloids; binary mixtures; Brownian dynamics

1. Introduction

In recent years, research has focused on the dynamics of crystal formation from an undercooled melt in order to identify the underlying molecular processes. This is important both from a fundamental point of view but also for many applications ranging from metallurgy [1], material science (e.g. for the formation of optical band-gap crystals) [2] to biology (e.g. for protein crystallization) [3–5]. In particular, real space information arising from computer simulations [6–10], density functional approaches [11,12] of model systems, phase field crystal calculations [13–16] and real-space experiments on colloidal dispersions [17–19] have elucidated the kinetic pathways of crystal nucleation and subsequent microstructure formation on the particle scale. Though more relevant for practical applications, heterogeneous crystal nucleation, which is initiated at impurities or system boundaries, is much less understood than homogeneous crystal nucleation in a bulk fluid [20,21]. Heterogeneous nucleation was studied for one-component systems (e.g. hard spheres,

two-dimensional dipoles) near smooth [7,22] or structured [23–26] walls, near external seed particles [27–29] or at imposed nucleation clusters [12]. However, quantitative and systematic studies on heterogeneous nucleation in two-component (binary) systems are sparse [30]. Binary systems have much more freedom for equilibrium crystal structures and therefore the heterogeneous crystallization is expected to be much richer: it depends critically on the thermodynamic parameters characterizing the bulk system *and* the structure of the external seed.

In this paper, we study heterogeneous crystallization near patterned walls in a two-dimensional model for binary dipolar colloidal suspensions. The particles interact via pairwise forces deriving from a repulsive potential of two parallel dipoles. This model is realized for superparamagnetic colloidal particles at a pending air–water interface in an external magnetic field which tunes the dipole moments [31–33] and the two-dimensional phase behaviour at zero temperature is known [34]. The formation of crystallites after a sudden increase of the field (corresponding to a fast

*Corresponding author. Email: messina@thphy.uni-duesseldorf.de

temperature quench) was explored in real-space experiments and compared to Brownian dynamics computer simulations [35]. Thereby, the formation of crystalline patches with different structures corresponding to stable and metastable phases was monitored as a function of time [35]. As a result, two-dimensional homogeneous crystallization after a fast quench exhibited a complex structure formation which involves disordered parts and crystallites. Apart from the thermodynamically stable structure, also metastable structures (such as triangles of big particles) were emerging as well [35]. On the time-scale explored by the experiment and the computer simulation, the thermodynamically stable crystalline state was not reached [35]. It is tempting to generalize these studies to heterogeneous crystallization since the (wall-free) behaviour is well characterized and can be used as a reference for comparison.

Here we study heterogeneous crystallization near patterned walls by extensive Brownian dynamics computer simulations. A similar setup for a one-component two-dimensional system was studied in [36]. The wall pattern exactly corresponds to the equilibrium crystal structure after the quench which is an alternating binary equimolar square crystal $S(AB)$. Two different wall patterns are considered which are composed of fixed particles forming a stripe of the stable square crystal. In principle, this can be realized experimentally by using optical tweezers. The walls are a cut through the $S(AB)$ crystal along the crystallographic (10)-direction where the outermost layer of fixed particle is either a row of big or small particles. (By ‘big’ or ‘small’ we refer to particles with a big or small dipole moment.) Since in both cases the wall structure imprints locally the equilibrium crystal, one would expect after a quench that heterogeneous crystallization near the walls is favoured and that crystallites with a metastable structure should be suppressed – relative to the unconfined case – at the walls. Contrarily we find that crystalline patches which involve big particles in a triangular structure are favoured near the wall with fixed outermost big particles. The concentration of big particles with a triangular crystalline neighbourhood is even larger than in the unconfined case. We attribute this unusual finding to pure kinetics of particle rearrangements after the quench, mainly governed by the much stronger AA interaction. It is not driven by energetics and therefore not simply contained in traditional classical nucleation theory [37,38].

In principle, our simulation results can be verified in real-space microscopy experiments of two-dimensional superparamagnetic particles [39–43] see also [44,45] for alternate set-ups. The immobile

particles building the external walls can be fixed by optical tweezers. Apart from that our results give more general insight into the molecular (i.e. particle-resolved) processes of heterogeneous crystallization, in particular at very fast and deep quenches where it competes with glass formation. Our findings demonstrate that the emergent behaviour is not controlled by equilibrium-like concepts (like line tensions) which form the basics of classical nucleation theory [46] but may be governed by local kinetics. This is expected to hold in a more general sense for any binary system when quenched quickly into a low-temperature state [47]. Our findings are also relevant for cooling-rate dependence of vitrification which competes with crystallization [10].

The paper is organized as follows: in Section 2, we describe the model and the simulation technique employed. In Section 3, we summarize the results and present snapshots and statistically averaged quantities after various quenches which reveal the heterogeneous crystallization behaviour. We devote Section 4 to a discussion and conclude in Section 5.

2. Model

The system consists of a suspension of two species of point-like super-paramagnetic colloidal particles denoted by A and B which are confined to a two-dimensional planar interface. Those particles are characterized by different magnetic dipole moments m_A and m_B , where $m = m_B/m_A$ is the dipole-strength ratio. The dipoles are induced by an external magnetic field H as $m_i = \chi_i H$ ($i = A, B$) where χ_i denotes the magnetic susceptibility. The magnetic field is applied perpendicular to the two-dimensional interface containing the particles. In the following the dipole-strength ratio m is fixed to 0.1 corresponding to recent experimental samples [35,41,42]. The relative composition $X = N_B/(N_A + N_B)$ of B particles is fixed at 50%, hence we are considering an equimolar mixture. The particles interact via a repulsive pair potential of two parallel dipoles of the form

$$u_{ij}(r) = \frac{\mu_0}{4\pi} m_i m_j / r^3 = \frac{\mu_0}{4\pi} \chi_i \chi_j H^2 / r^3 \quad (i, j = A, B), \quad (1)$$

where r denotes the distance between two particles. For this inverse power potential, at fixed composition X and susceptibility ratio χ_B/χ_A , all static quantities depend solely [48] on a dimensionless interaction strength (or coupling constant)

$$\Gamma = \frac{\mu_0 \chi_A^2 H^2}{4\pi k_B T a^3}, \quad (2)$$

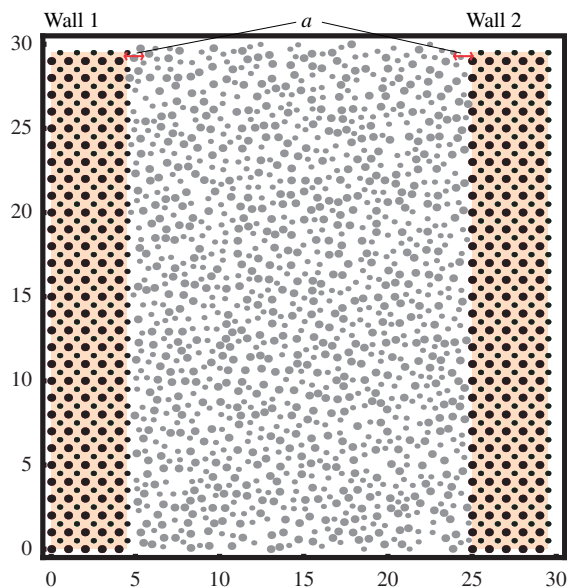


Figure 1. Schematic illustration of colloidal particles confined between two walls at $\Gamma_{\text{init}} = 0$ with a finite particle wall interaction. The big circles (small) represent A-particles (B-particles). The fixed particles are indicated by black full circles and are backed by orange ground. All other large particles are shown in grey. The distance a represents the average interparticle separation between big particles. The two different wall structures are referred to as wall 1 (left wall, where the outermost layer consists of fixed small particles) and wall 2 (right wall, where the outermost layer consists of fixed big particles).

where $k_B T$ is the thermal energy and $a = 1/\rho_A^{1/2}$ the average interparticle separation between A particles. Here, ρ_A denotes the areal number density of the A particles.

We perform non-equilibrium Brownian dynamics (BD) computer simulations [49,50]. Hydrodynamic interactions are neglected. The Brownian time scale is set by the short-time diffusion constant D_A of the A particles. Knowing that this diffusion constant scales with the inverse of the radius of a particle, D_B was chosen such that $D_B/D_A = 1.7$ corresponding to the physical diameter ratio of the experimental samples [35,41,42]. A finite time step $\delta t = 10^{-5}\tau$, where $\tau = a^2/D_A$, was used in the simulations.

Two different wall patterns consist of fixed particles belonging to a crystalline centred square structure. These walls are chosen with a finite width of $20a$ and periodic boundary conditions are applied in both directions. A simulation box set-up is sketched in Figure 1. The black-coded particles indicate the fixed A and B particles which belong to square clusters. The outermost row of wall 1 (left wall in Figure 1) is composed of small particles. On the other hand, big particles form the outermost row of wall 2

(right wall in Figure 1). $N_A = 900A$ particles and $N_B = 900B$ particles were placed in a square box including the fixed wall particles. As a reference, we have also performed simulations in a square simulation box with periodic boundary conditions in the absence of any walls with the same number of particles.

Starting from an initial configuration of non-interacting particles which initially do not penetrate the walls (see the snapshot in Figure 1) we have changed the coupling Γ as a function of time by changing the magnetic field (while keeping the densities and the temperature fixed). This corresponds formally to a cooling process. The cooling history is as follows: first we increase the interaction strength Γ by constant steps of $d\Gamma = 5$ and within a time $\Delta t = 1\tau$ to let the system equilibrate. This procedure is continued until a prescribed coupling Γ_{init} (initial coupling) is reached. From this configuration, a sudden quench is performed to $\Gamma = \infty$ (i.e. the temperature is set to zero leading to a steepest descent quench). The time for the instantaneous quench sets the zero on our time axis. We checked that the initial state with $\Gamma = \Gamma_{\text{init}}$ was equilibrated enough. Details of the cooling history are shown in Figure 2. Finally we averaged over 10 different starting configurations in order to reduce the statistical error.

Our aim is to study crystal nucleation near the walls after the sudden quench. Therefore we have used criteria to define A particles which have a pure triangular surrounding of other A particles, i.e. which are close to a cut-out of a pure triangular A crystal, and, likewise, we have identified A and B particles which form locally an equimolar square lattice $S(AB)$. The corresponding two structure elements are shown as insets in Figure 2. Following the definition used in [41], in detail, we associate a triangular surrounding to an A particle if the following two criteria are fulfilled simultaneously: (i) the six-fold bond order parameter $p_6 = (\Psi_6^* \Psi_6)^{1/2}$ (where $\Psi_6 = \frac{1}{6} \sum_{\text{NN}} \exp(i6\theta_{\text{NN}})$ with θ_{NN} denoting the angles of the six nearest neighbour bonds relative to a fixed reference) is larger than 0.94. (ii) The relative bond length deviation $b_6 = \frac{1}{6} \sum_{\text{NN}} [(l_{\text{NN}} - \bar{l})/\bar{l}]$, where \bar{l} is the average length of the six bond lengths l_{NN} , is smaller than 0.04. This double condition selects local configurations close to those of a perfect triangular lattice where p_6 is unity and b_6 vanishes. Likewise we define a square surrounding around a B particle by the criteria: (i) the four-fold bond order parameter $p_4 = (\Psi_4^* \Psi_4)^{1/2}$ (where $\Psi_4 = \frac{1}{4} \sum_{\text{NN}} \exp(i4\theta_{\text{NN}})$ with θ_{NN} denoting the bond angles of the four nearest neighbour AB bonds) is larger than 0.92. (ii) The corresponding relative AB bond length deviation b_4 is smaller than 0.05.

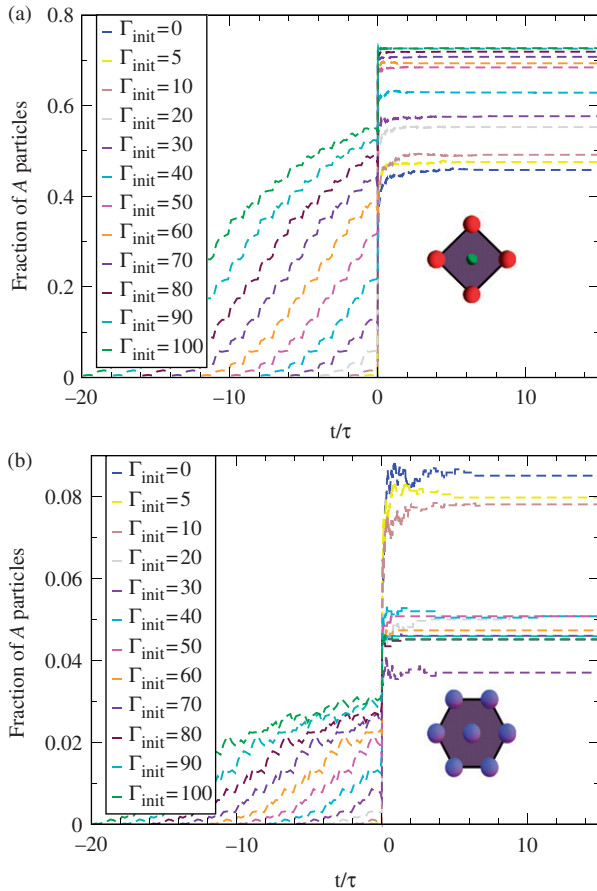


Figure 2. (a) Fraction of A particles belonging to a crystalline square (see inset) and (b) fraction of A particles belonging to a crystalline triangular surrounding (see inset) versus reduced time t/τ for instantaneous ‘steepest descent’ quench from different Γ_{init} to $\Gamma = \infty$ in the unconfined case. For negative times, the system is slowly cooled until reaching Γ_{init} for $t = 0$. Details of the stepwise cooling history are given in the text. Then the system is instantaneously brought to $\Gamma = \infty$ at $t = 0$. Different colours correspond to different Γ_{init} , see legend.

3. Results

Figure 2(a) and (b) refer to the unconfined case in the absence of walls. The fraction of A particles with a triangular and with a square surrounding as a function of time is displayed, respectively, for different Γ_{init} . The average here is over all mobile A particles of the system. First the cooling preparation can be seen, shown for negative times in Figure 2. The particle number is increasing with time as the coupling is stepwise increased. After each increase the system equilibrates. This has been checked by taking slower cooling rates where relaxation time after each cooling step is doubled which did not affect the data. Hence, at different Γ_{init} , the system is pre-ordered containing already a small amount of crystallites with square and

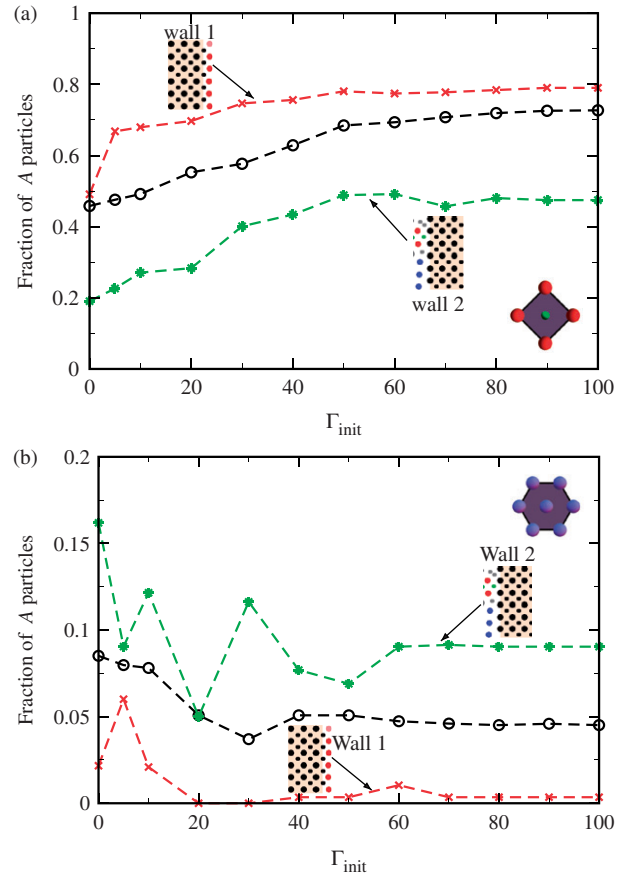


Figure 3. (a) Fraction of A particles belonging to a crystalline square surrounding (see inset) and (b) fraction of A particles belonging to a crystalline triangular surrounding (see inset) versus Γ_{init} 15τ after the quench. Red line: within a stripe of width a near wall 1, green line: within a stripe of width a near wall 2, black line: in the unconfined case (as a reference).

triangular local ordering. After the sudden quench (performed at $t = 0$), the number of crystalline particles is steeply increasing first and then saturates on the time-scale of 15τ explored by the simulation. This latter feature is precisely addressed in Figure 3. In general there are less particles with triangular order than those with square order (see the different scales in Figure 2a and b). Therefore the data on the triangular particles are more noisy in general.

In general, there is an opposite trend of the number of square and triangular crystallites with Γ_{init} : while the number of square particles is growing with Γ_{init} , the number of triangular particles is decreasing with Γ_{init} . This has to do with the fact that there is pre-ordering in the fluid state which corresponds to the thermodynamically stable ground state $S(AB)$. Hence an equilibrated highly correlated fluid state is quenched more

easily into crystalline patches with square-like symmetry. Conversely, the triangular structure is occurring most in uncorrelated systems upon a sudden cooling process. However, there is a minimal number of triangular particles for $\Gamma_{\text{init}} = 30$ which possibly is within the statistical accuracy (see also data for the unconfined case in Figure 3b).

We now address the question of how the walls influence the local occurrence of crystallites relative to their formation in the unconfined case. Reference data with the same cooling history but in a system without any walls are produced similar to that shown in [35]. In order to monitor the crystallites close to the walls we have defined a strip of width a parallel to the wall and count only particles within this strip. The relative fraction of A-particles with triangular or square ordering within this strip indicates the amount of heterogeneous crystallization near the walls. This quantity is shown in Figure 3(a) and (b) as a function of the initial coupling Γ_{init} 15τ after the quench together with the wall-free data as a reference. As expected, the fraction of particles with a square-like surrounding depicted in Figure 3(a) is increasing with Γ_{init} . Close to wall 1, there are more such particles than in the unconfined case which is understood by the fact that wall 1 induces square like ordering into the adjacent fluid mixture. However, although wall 2 is also imprinting the same square-like structure into the fluid, there are fewer of these particles at wall 2 than in the unconfined case. This is most pronounced for small Γ_{init} but still significant at high Γ_{init} . Conversely, the number of triangular particles at wall 1 is much lower than in the unconfined case while at wall 2 this number is definitely higher than in the unconfined case, see Figure 3(b). The large fluctuations have to do with the limited set of 10 different initial configurations used for the average. Still the absolute fraction is such that there are more square-like particles than triangular-like particles (compare the different scales of Figure 3a and b). It is only for wall 2 at low Γ_{init} that these two numbers are comparable.

Actual particle snapshots after the quench are shown in Figure 4 for $\Gamma_{\text{init}} = 0$ and $\Gamma_{\text{init}} = 100$ with appropriately colour-coded particles indicating the locations of A and B particles which belong to local triangular and square clusters. If an A particle has a triangular surrounding, all seven A particles including the central one with its full surrounding are shown in blue. Conversely, if a B particle has a square surrounding, it is coloured in green and its four A neighbours are coloured in red. All particles which belong both to the blue and the red class are shown in pink. In consistence with Figure 2, the crystalline clusters grow as a function of Γ_{init} . What can be deduced from the snapshots is that

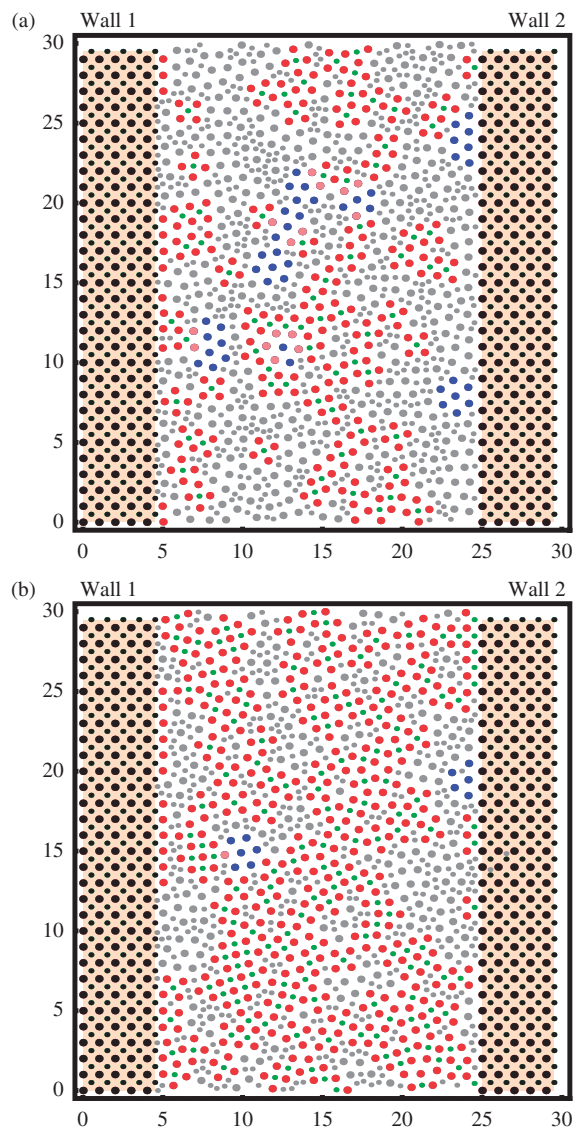


Figure 4. Simulation snapshots 15τ after the instantaneous quenching process for (a) $\Gamma_{\text{init}} = 0$ and (b) $\Gamma_{\text{init}} = 100$. Big particles are shown in blue if they belong to a triangular surrounding and in red if they belong to a square surrounding. The black full circles indicate fixed particles and all other large particles are shown in grey.

the actual particle clusters are small. On the time-scale of the simulation they are fluctuating a bit, but are not significantly growing in size. Hence on the observation time-scale the system is far away from the thermodynamically stable state of a perfect square crystal between the two walls.

4. Discussion

In the unconfined case, the stable state (or ground state) after a steepest descent quench is the stable

crystalline lattice which minimizes the total potential energy at fixed composition. In our previous work [34], it was shown that the stable state is a square $S(AB)$ crystal which exactly coincides with the boundaries assumed in our simulation. Therefore the interfacial energy between this (wall-free) phase and the imposed boundary is zero. Moreover the spacing between the two walls allows an exact match of the $S(AB)$ crystal. This implies that the stable confined state is a strip (cutout) of the $S(AB)$ crystal. Hence the exact state is known and, given enough time and enough fluctuations, the system should reach this state after the quench. Moreover, the fixed boundaries in fact favour locally a (10)-oriented $S(AB)$ crystal. Therefore one expects that near the walls the $S(AB)$ crystalline structure is enhanced relative to its occurrence in the unconfined case, i.e. that the $S(AB)$ crystal will heterogeneously nucleate at the walls.

Strikingly, after a sudden quench, as realized in our simulations, the system does not relax into the true ground state and even avoids the preferential $S(AB)$ structure near wall 2 where the outermost layers are fixed big (A) particles. Instead, locally a triangular crystal of pure A particles is preferentially nucleated near wall 2 (even compared to the wall-free case as a reference). Near wall 1, on the other hand, the behaviour is more like expected: here, more square-like A particles are showing up than in the unconfined case, pointing to the locally preferred $S(AB)$ crystal. The counter-intuitive behaviour near wall 2 has to do with the very fast quench. A simple argument goes along the following line: for a sudden quench first the big A particles relax near a wall which is made by fixed A particles only. Therefore, neglecting all small particles in the fast process of reordering, the big particles try to arrange in a triangular cluster and freeze in. Near wall 2, on the other hand, there is a fine structure of the outermost fixed small particles which locally forbids a triangular structure of the big particles. Clearly, classical nucleation theory, which is formulated in terms of interfacial tensions, would not predict the nucleation of triangular particles near wall 2. The failure of classical nucleation theory [37,38] has to do with the rapid quench which violates the inherent conditions of local thermodynamic equilibrium.

However, the general scenario is compatible with the traditional Ostwald's step rule [51–53] of homogeneous nucleation which tells that if an unstable phase A transforms into a stable phase B , a metastable phase C can intervene if it is 'kinetically more accessible' than phase B . In many (but not all) applications of the Ostwald's step rule a finite sheet of the metastable phase C even remains in equilibrium coexistence between phases A and B . In this case, the equilibrium

interfacial tension between A and B is minimized via the intervening layer of C . In our case, the phases A and B are identical and hence an intervening layer in equilibrium is prohibited. Hence the occurrence of the triangular crystallites is completely due to kinetics.

5. Conclusion

In conclusion, we have studied heterogeneous crystallization near patterned walls by extensive Brownian dynamics computer simulations. The wall pattern corresponds exactly to the equilibrium crystal structure after the quench which is an alternating binary equimolar square crystal $S(AB)$. Two different wall patterns are considered (wall 1 and wall 2) which are made up by fixed particles forming a stripe of the stable square crystal. Since in both cases the wall structure imprints locally the equilibrium crystal, one would expect after a quench that heterogeneous crystallization near the walls is favoured and that crystallites with a metastable structure should be suppressed – relative to the unconfined case – at the walls. Contrarily we find that crystalline patches which involve big particles in a triangular structure are favoured near wall 2 with fixed outermost big particles even relative to the unconfined case. We attribute this to pure kinetics of particle rearrangements after the rapid quench. It is therefore not contained in traditional classical nucleation theory [37,38].

In principle, our set-up studied can be realized experimentally by using optical tweezers in order to fix the wall particles. Real-space microscopy experiments of two-dimensional superparamagnetic particles are quite common for binary mixtures and have been used to study the dynamics after a quench into the glass [39–43]. Our results provide also more general insight into the molecular (i.e. particle-resolved) processes of heterogeneous crystallization, in particular at very fast and deep quenches where it competes with glass formation. In fact, our findings demonstrate that the emergent behaviour is not controlled by equilibrium-like concepts (like line tensions) which form the basics of classical nucleation theory [46] but may be governed by local kinetics. This is expected to hold in a more general sense for any binary system when quenched quickly into a low-temperature state [47]. Our findings are therefore also relevant for the general relation between crystallization and vitrification [54–56].

Acknowledgements

We dedicate this paper to R. Evans who is one of the pioneers of statistical mechanics of confined systems. This work was financially supported by the DFG within SPP 1296.

References

- [1] H. Emmerich, K. Binder and B. Nestler, *Phil. Mag. Lett.* **87**, 791 (2007).
- [2] N.V. Dziomkina and G.J. Vancso, *Soft Matter* **1**, 265 (2005).
- [3] M.C. Wiener, *Methods* **34**, 364 (2004).
- [4] E.H. Snell and J.R. Helliwell, *Rep. Prog. Phys.* **68**, 799 (2005).
- [5] R. Sear, *J. Phys.: Condens. Matter* **19**, 033101 (2007).
- [6] S. Auer and D. Frenkel, *Adv. Polym. Sci.* **173**, 149 (2005).
- [7] A. Cacciuto and D. Frenkel, *Phys. Rev. E* **72**, 041604 (2005).
- [8] C. Desgranges and J. Delhommelle, *J. Chem. Phys.* **126**, 054501 (2007).
- [9] T. Schilling, H.J. Schöpe, M. Oettel, G. Opletal and I. Snook, *Phys. Rev. Lett.* **105**, 025701 (2010).
- [10] H. Shintani and H. Tanaka, *Nat. Phys.* **2**, 200 (2006).
- [11] R. Ohnesorge, H. Löwen and H. Wagner, *Phys. Rev. A* **43**, 2870 (1991).
- [12] S. van Teeffelen, C.N. Likos and H. Löwen, *Phys. Rev. Lett.* **100**, 108302 (2008).
- [13] H. Emmerich, *Adv. Phys.* **57**, 1 (2008).
- [14] L. Gránásy, T. Pusztai and J.A. Warren, *J. Phys.: Condens. Matter* **16**, R1204 (2004).
- [15] L. Gránásy, T. Pusztai, T. Börzsönyi, G. Tóth, G. Tegze, J.A. Warren and J.F. Douglas, *J. Mater. Res.* **21**, 309 (2006).
- [16] L. Gránásy, T. Pusztai, D. Saylor and J.A. Warren, *Phys. Rev. Lett.* **98**, 035703 (2007).
- [17] U. Gasser, *J. Phys.: Condens. Matter* **21**, 203101 (2009).
- [18] U. Gasser, E.R. Weeks, A. Schofield, P.N. Pusey and D.A. Weitz, *Science* **292**, 258 (2001).
- [19] C.P. Royall, S.R. Williams, T. Ohtsuka and H. Tanaka, *Nat. Mater.* **7**, 556 (2008).
- [20] H. Emmerich, *J. Phys.: Condens. Matter* **21**, 460301 (2009).
- [21] G. Kahl and H. Löwen, *J. Phys.: Condens. Matter* **21**, 464101 (2009).
- [22] P. Wette, A. Engelbrecht, R. Salh, I. Klassen, D. Menke, D.M. Herlach, S.V. Roth and H.J. Schöpe, *J. Phys.: Condens. Matter* **21**, 464115 (2009).
- [23] M. Heni and H. Löwen, *Phys. Rev. Lett.* **85**, 3668 (2000).
- [24] M. Heni and H. Löwen, *J. Phys.: Condens. Matter* **13**, 4675 (2001).
- [25] W.S. Xu, Z.Y. Sun and L.J. An, *J. Chem. Phys.* **132**, 144506 (2010).
- [26] S. van Teeffelen, H. Löwen, R. Backofen and A. Voigt, *Phys. Rev. E* **79**, 051404 (2009).
- [27] V.W.A de Villeneuve, R.P.A Dullens, D.G.A.L. Aarts, E. Groeneveld, J.H. Scherff, W.K. Kegel and H.N.W Lekkerkerker, *Science* **309**, 1231 (2005).
- [28] V.W.A de Villeneuve, D. Verboekend, R.P.A Dullens, D.G.A.L. Aarts, W.K. Kegel and H.N.W Lekkerkerker, *J. Phys.: Condens. Matter* **17**, S3371 (2005).
- [29] A. Cacciuto, S. Auer and D. Frenkel, *Nature* **428**, 404 (2004).
- [30] S.R. Williams, C. Royall and G. Bryant, *Phys. Rev. Lett.* **100**, 255502 (2008).
- [31] N. Hoffmann, F. Ebert, C.N. Likos, H. Löwen and G. Maret, *Phys. Rev. Lett.* **97**, 078301 (2006).
- [32] L. Assoud, F. Ebert, P. Keim, R. Messina, G. Maret and H. Löwen, *J. Phys.: Condens. Matter* **21**, 464114 (2009).
- [33] Y. Terada and M. Tokuyama, *J. Phys. Soc. Jpn.* **79**, 034802 (2010).
- [34] L. Assoud, R. Messina and H. Löwen, *Europhys. Lett.* **80**, 48001 (2007).
- [35] L. Assoud, F. Ebert, P. Keim, R. Messina, G. Maret and H. Löwen, *Phys. Rev. Lett.* **102**, 238301 (2009).
- [36] K. Franzrahe, P. Nielaba, A. Ricci, K. Binder, S. Sengupta, P. Keim and G. Maret, *J. Phys.: Condens. Matter* **120**, 404218 (2008).
- [37] T. Young, *Trans. Roy. Soc. London* **95**, 65 (1805).
- [38] R. W. Cahn and P. Haasen, *Physical Metallurgy* (North Holland, Amsterdam, 1983).
- [39] M. Kollmann, R. Hund, B. Rinn, G. Nagele, K. Zahn, H. König, G. Maret, R. Klein and J.K.G Dhont, *Europhys. Lett.* **58**, 919 (2002).
- [40] H. König, R. Hund, K. Zahn and G. Maret, *Eur. Phys. J. E* **18**, 287 (2005).
- [41] F. Ebert, P. Keim and G. Maret, *Eur. Phys. J. E* **26**, 161 (2008).
- [42] S. Mazoyer, F. Ebert, G. Maret and P. Keim, *Europhys. Lett.* **88**, 66004 (2009).
- [43] F. Ebert, G. Maret and P. Keim, *Eur. Phys. J. E* **29**, 311 (2009).
- [44] A. Pertsinidis and X.S. Ling, *Nature* **413**, 147 (2001).
- [45] Z.R. Wang, A.M. Alsayed, A.G. Yodh and Y.L. Han, *J. Chem. Phys.* **132**, 154501 (2010).
- [46] L. Granasy and P.F. James, *J. Non-Cryst. Solids* **253**, 210 (1999).
- [47] V.A. Shneidman and D.R. Uhlmann, *J. Chem. Phys.* **108**, 1094 (1998).
- [48] J.-P. Hansen and I.R. MacDonald, *Theory of Simple Liquids*, 2nd ed. (Academic, New York, 1986).
- [49] M.P. Allen and D.J. Tildesley, *Computer Simulation of Liquids* (Oxford Science Publications, New York, 1987).
- [50] For an equilibrium molecular dynamics simulation for a similar model, see T. Stirner and J. Sun, *Langmuir* **21**, 6636 (2005).
- [51] W. Ostwald, *Z. Phys. Chem.* **22**, 289 (1897).
- [52] J. Bechhoefer, H. Löwen and L.S. Tuckerman, *Phys. Rev. Lett.* **67**, 1266 (1991).
- [53] P.R. ten Wolde and D. Frenkel, *Phys. Chem. Chem. Phys.* **1**, 2191 (1999).
- [54] T. Kawasaki and H. Tanaka, *Proc. Natl. Acad. Sci. USA* **107**, 14036 (2010).
- [55] E. Zaccarelli, C. Valeriani, E. Sanz, W.C.K Poon, M.E. Cates and P.N. Pusey, *Phys. Rev. Lett.* **103**, 135704 (2009).
- [56] T. Palberg, A. Stipp and E. Bartsch, *Phys. Rev. Lett.* **102**, 038302 (2009).